Int. J. Multiphase Flow Vol. 19, No. 3, pp. 439–450, 1993
Printed in Great Britain

0301-9322/93 $6.00 + 0.00
Pergamon Press Ltd

EXPERIMENTAL INVESTIGATIONS ON BUBBLY FLOWS IN A STRAIGHT CHANNEL ROTATED AROUND AN AXIS PERPENDICULAR TO THE CHANNEL

K. MINEMURA,[1] T. UCHIYAMA[1] and T. ISHIKAWA[2]
[1]College of General Eduction, Nagoya University, Nagoya 464-01, Japan
[2]Toyota Motor Co. Ltd, Toyota 471, Japan

(Received 17 September 1992; in revised form 18 February 1993)

Abstract—This paper describes experimental investigations on the behavior of an air–water two-phase mixture in a horizontal, radial-flow and square-sectioned straight channel, which rotates around an axis perpendicular to the channel. The hydraulic loss of head and the distributions of pressures and void fractions in the channel were measured mainly in a bubbly flow regime, and the effects of the rotating speed of the channel and the flow rate of water on the loss were discussed in relation to the inlet void fraction. When the rotating speed is increased or the flow rate of water is decreased, a predominant region of high void fractions appearing on the downstream negative side tends to expand upstream as the Rossby number is increased. An almost imperceptible pressure rise in the radial direction of this region causes an excessive increase in the hydraulic loss.

Key Words: bubbly flow, rotating channel, pressure distribution, void fraction, Rossby number

1. INTRODUCTION

Although most hydraulic turbo-machinery is originally designed for handling single-phase liquid flows, it is frequently operated under gas–liquid two-phase flow conditions. In such cases its performance generally deteriorates, depending on the circumstances. It is, therefore, practically important to know the behavior of mixtures in rotating fields and to establish methods to predict the flow characteristics and design the optimal machinery configuration.

Minemura & Murakami (1988) have been studying the performance of centrifugal pumps of various specific speeds, mainly under a bubbly flow regime. They have found that performance is closely related to the flow patterns in the impeller. With the intention of clarifying the rotating effect of the flow field on the two-phase flow behavior in a simpler system than such practical flow channels, the flows in a radially uniform square-sectioned channel, which rotates around an axis perpendicular to the channel, were observed by Patel & Runstadler (1978) and numerically analyzed based on the one-dimensional theory of Zakem (1980a, b), both mainly under a bubbly flow regime. In their investigations, changes in the flow pattern and relative velocity between the two phases were discussed in relation to the volumetric flow rate of the liquid phase. Under single phase flow conditions, the flows in such a rotating channel are characterized by the Rossby number (Murakami & Kikuyama 1972), which is the ratio of the Reynolds number for the flow velocity to that for the rotating speed. Even in two-phase flow conditions, the Rossby number should figure importantly, but the observations and calculations to date have not taken the Rossby number into consideration. Thus, the flows in the channels have been compared with those in an impeller having a very different Rossby number. In two-phase flow conditions, the flow characteristics are further complicated by the uneven distribution of the void fractions in the cross sections. Thus, the results of such observations and calculations cannot predict the true nature of the two-phase flows in pump impellers.

To clarify the problems mentioned above, the flows in a rotating radial channel with a square section were experimentally investigated in this study, and distributions of pressures and void fractions were measured mainly under a bubbly flow regime. The resultant hydraulic loss was discussed in relation to the rotating speed and the velocity of the liquid phase, namely the Rossby number, as well as the volumetric flow ratio of air to water and the flow patterns. The channel is mounted on a horizontal disk rotated around an axis perpendicular to the channel, and the mixture flows in an outward radial direction from the center.

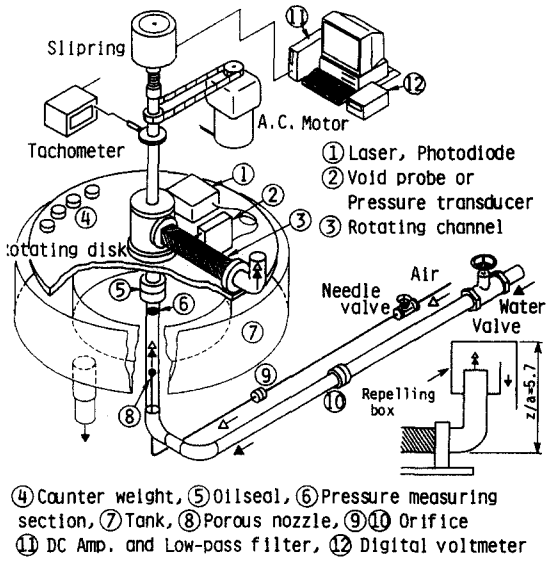

Figure 1. Layout of the experimental apparatus.

2. EXPERIMENTAL APPARATUS AND PROCEDURE

2.1. Experimental apparatus

Figure 1 shows the general arrangement of the experimental apparatus. A square-sectioned straight channel ③, made of transparent Plexiglas, is mounted radially on a horizontal disk and rotated with the disk around its vertical axis. Water from a reservoir tank enters a vertically running pipe through a regulating valve and an orifice to measure the water flow rate ⑩. Air from a compressor is led, through a regulating valve and a metering orifice ⑨, to the pipe at an elevation $z/a = -15$, where the elevation from the bottom surface of the rotating channel z is non-dimensionalized by the width of the square channel a. The air is mixed with the water through a porous nozzle ⑧ to generate a homogeneous flow with fine bubbles. The stationary pipe is connected through an oil-seal ⑤ with a rotating vertical pipe, the axis of which coincides with that of the rotating disk. The flow in the pipe is horizontally directed by an elbow and introduced to the rotating straight channel ③, in which the distributions of the pressures and void fractions were measured. Downstream of the channel the mixture is released in the air through an elbow into a water collector tank ⑦. The way the elbow is directed upward or downward would obviously affect the flow behavior, so experiments in both directions were performed. When the system discharge is upward, the mixture is guided into the tank by a repelling box, by which the exit water level was maintained almost unaltered ($z/a = 5.7$). To measure the pressure rise in the rotating channel, the inlet static pressure on the stationary pipe wall, slightly upstream of the oil-seal ($z/a = -6.7$), was measured at openings over the pipe cross section and then averaged with the aid of a ring manifold.

The rotating channel shown in figure 2 is a square-sectioned straight straight pipe measuring 283 mm long and 32 mm wide, with both ends connected to a 32 mm dia vertical pipe through an elbow. To minimize hydraulic losses in these connecting lines, the shape of the portion between the inlet elbow and the inlet of the square channel, $0.061 \leqslant r/r_3 \leqslant 0.134$, undergoes a gradual transition from a circular to a square section, and that between the channel and the outlet elbow, $0.785 \leqslant r/r_3 \leqslant 0.854$, changes from a square to a circular section. The radial coordinate r is denoted non-dimensionally by the outlet radius of the rotating channel r_3.

2.2. Experimental conditions

In this study, flows in the rotating channel were measured mainly under a bubbly flow regime. The experimental conditions were as follows: the rotating speeds of the channel ranged from 0 to 110 rpm; the volumetric flow rates of water ranged from 0.042 to 0.074 m^3/min; and the volumetric flow ratio of air to whole fluid in the inlet section of the rotating pipe lines, ϵ_0, ranged from 0 to

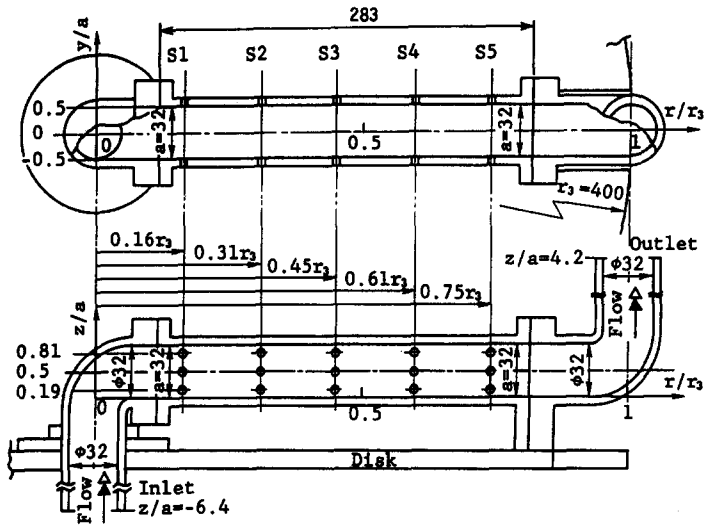

Figure 2. Shape and dimensions of the rotating straight channel.

0.08. Strobolight observations made it possible to achieve almost uniform dispersion of fine bubbles with 1–2 mm dia (i.e. bubbly flow condition) in the vertically running pipe under the above conditions.

2.3. Measurement of the pressure distribution

Wall pressures on the front and back sides of the rotating channel were measured at three sections with different elevations from the bottom of the channel ($z/a = 0.19, 0.5, 0.81$) and at five positions (S1–S5) in the radial direction, at a total of 15 measuring points as shown in figure 2. The pressures were detected with semi-conductive pressure sensors through narrow openings, 0.5 mm dia, drilled in the walls. Electrical signals obtained by the sensors were transmitted to a signal processing unit in a stationary system through slip-rings. In consideration of noise, the average of 5 measurements was employed for the pressure.

2.4. Measurement of the void fraction distribution

The local void fraction ϵ was measured with a single optical fiber probe, so that the flow would not be affected by other probes. The probe was inserted into the openings for measuring wall pressures and traversed in the channel-width direction under remote control from the stationary system to measure the void fraction distributions. The measuring system consists of a semi-conductive laser (15 mW), optical fibers (ϕ0.14) and the photodiode illustrated in figure 3. The tail end of the fiber was polished at an angle of 45° and its lateral side was coated with nickel. The fiber was bonded to a 0.7 mm dia support tube made of stainless steel, with a 10 mm length exposed, so that the flow behind it would not be disturbed by the support and the possible fiber vibration due to the flow. It is only when the slanted fiber end is in the gas phase that the supplied laser beam is reflected and develops an output voltage to the photodiode. The output was transmitted

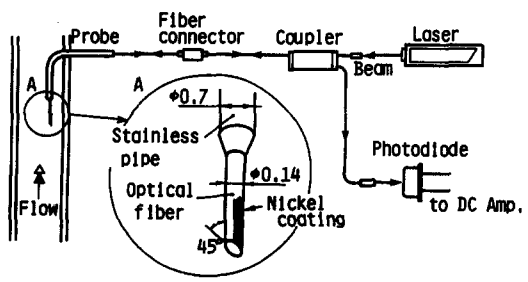

Figure 3. Measuring system of the optical fiber probe.

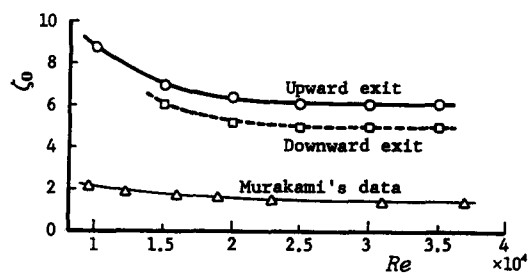

Figure 4. Friction factor of single-phase water flow in the stationary channel.

to the stationary system through the slip-rings and processed by sampling after amplification. The local void fraction was here defined to be the ratio of the time the gas phase was present over the probe to the total duration of the experiment (5 s), and the averaged value of ϵ was used after 5 measurements. Since the wave forms of the output voltage obtained were virtually rectangular, the results were hardly affected by the threshold value when distinguishing between gas and liquid phases.

2.5. Definition of pressure losses

If a homogeneous flow model, which postulates no slip between two phases and homogeneously dispersed gas phase, is applied to the bubbly flow in a channel rotating with a constant angular velocity ω, the conservation law of energy for a steady-state condition can be expressed by the sum of the changes in energy of the mixture and the loss of pressure Δp_{tp} between the inlet and outlet of the channel as

$$\int_{s_0}^{s_3}\left[\rho_{tp}W_{tp}\left(\frac{dW_{tp}}{ds}\right)-\rho_{tp}r\omega^2\left(\frac{dr}{ds}\right)+\left(\frac{dp}{ds}\right)+\rho_{tp}g\right]ds+\Delta p_{tp}=0, \quad [1]$$

where the density ρ_{tp}, the relative velocity W_{tp} and the pressure p under two-phase flow conditions, are the respective mean values over the channel cross section, and g and s denote the acceleration of gravity and the streamline coordinate, respectively. The subscripts 0 and 3 indicate the inlet and outlet of the rotating channel, respectively.

Using integration by parts for the first term, [1] is reduced to

$$\left[\rho_{tp}\frac{W_{tp}^2-u^2}{2}+p+\rho_{tp}gz\right]_0^3-\int_{s0}^{s_3}\left(\frac{W_{tp}^2-u^2}{2}\right)\left(\frac{d\rho_{tp}}{ds}\right)ds+\Delta p_{tp}=0, \quad [2]$$

where u is the peripheral speed of the rotating channel and z is the elevation from the bottom surface of the channel.

In this experiment the pressure change from p_0 at the inlet to p_3 at the outlet is very small and $p_0/p_3=1.04$, even if the maximum is attained. The corresponding change in the density ρ_{tp} is also slight. Thus, let the density be constant; then Δp_{tp} can be expressed from [2] by the following equation:

$$\Delta p_{tp}=\rho_{tp}g\left[\frac{u_3^2-u_0^2}{2g}-\frac{W_{tp3}^2-W_{tp0}^2}{2g}-\frac{p_3-p_0}{\rho_{tp}g}-(z_3-z_0)\right]. \quad [3]$$

When a single-phase liquid with density ρ_L flows, the loss of pressure Δp is related to the velocity head and characterized by a friction factor. With the mean velocity in the channel W, the friction factor for the rotating channel ζ can be given by

$$\zeta\equiv\frac{\dfrac{\Delta p}{\rho_L g}}{\dfrac{W^2}{2g}}. \quad [4]$$

Under two-phase flow conditions, the loss is expressed as the pressure-loss multiplier ϕ_L, and is defined here by the ratio of the pressure loss in the two-phase flow Δp_{tp} to that in the single-phase liquid flow Δp_L under the same mass flow rate:

$$\phi_L\equiv\left(\frac{\Delta p_{tp}}{\Delta p_L}\right)^{1/2}. \quad [5]$$

To obtain the pressure distributions in a radial direction, the static pressure p measured on the side walls of the mid-section ($z/a=0.5$) between the top and bottom of the channel is referred to the wall value p_0 at the stationary pipe just upstream of the rotating channel ($z/a=-6.7$), and its dimensionless value $\Delta\psi_r$ is expressed as

$$\Delta\psi_r=\frac{p-(p_0-\rho_{tp}g\,\Delta z)}{\rho_L u_3^2}. \quad [6]$$

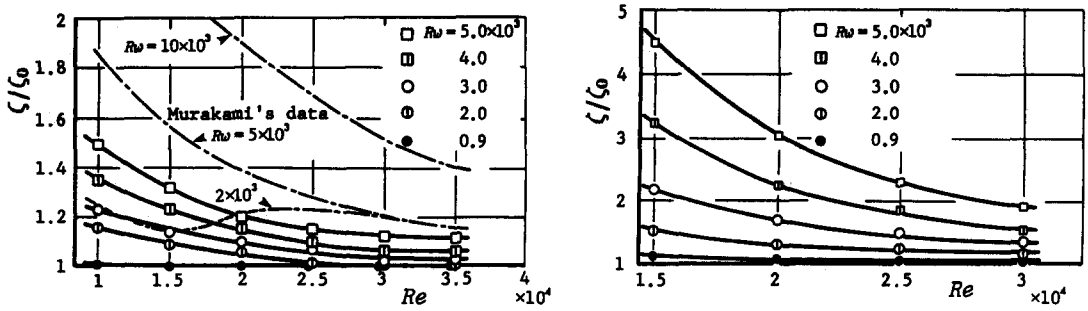

Figure 5. Friction factor of single-phase water flow in the rotating channel: (a) upward exit; (b) downward exit.

2.6. Dimensionless numbers

As a dimensionless number expressing the angular velocity of the channel ω, a Reynolds number for the rotating speed is used here as Rw ($= \omega a^2/2\nu$; a is the width of the square channel; ν is the kinematic viscosity of water), which corresponds, in due consideration of the liquid phase as the continuum medium, to the ratio of the Coriolis force to the viscous force acting on a unit volume of the liquid phase. As a dimensionless number for the flow rate, a relevant Reynolds number for the superficial liquid velocity W_L is used as Re ($= aW_L/\nu$), when it is assumed that the liquid phase alone flows even in two-phase flow conditions. In this case the Rossby number Ro, the ratio of the inertial force to the Coriolis force, is given by the ratio of Re to Rw, i.e. $\mathrm{Ro} = 2W_L/a\omega$. The value of Ro for radial-flow pumps of low specific speed, in general, is $0.05 < 1/\mathrm{Ro} < 1$ under the rated flow condition.†

3. EXPERIMENTAL RESULTS AND DISCUSSION

3.1. Hydraulic loss in single-phase water flow

When a liquid flows in stationary pipes, its friction factor ζ_0 depends on Re. Such a dependence for the channel employed in this experiment is shown in figure 4, where the results for the channel with upward and downward exits are plotted by the symbols ○ and □, respectively. Both values of ζ_0 decrease similarly with an increase in Re and become constant in the range $\mathrm{Re} \geqslant 2.5 \times 10^4$. The channel with a downward exit has less loss, which is probably attributable to less interference of secondary flows. Even when the fluid flows into the inlet elbow with a uniform velocity, the axial component of the velocity behind the elbow becomes higher toward the outside of the curvature due to the secondary flow, and the fluid flows rectilinearly into the outlet elbow with this distribution. When the exit elbow is oriented downward, therefore, the higher velocity component flows into the exterior curvature of the outlet elbow and counterbalances the effect of the secondary flow. But the channel with an upward exit presents the opposite case.

Figure 4 also includes the results for a U-shaped return-bend with a circular section, measured earlier by Murakami & Kikuyama (1972). The bend has an additional return pipe to the present channel and a greater radius of curvature, $R/a = 1.44$, where R is the radius of curvature of the bend and inlet and outlet elbow, and a is the pipe diameter. The greater elbow radius results in much smaller ζ_0, owing to the smaller effect of the secondary flow. For the present channel, $R/a = 0.5$, which apparently corresponds to that of radial-flow pumps.

When the channel is rotating, the loss ζ decreases with an increase in Re as shown in figure 5(a), where the results for the channel with the upward exit are expressed dimensionlessly by that for the stationary pipe ζ_0 as ζ/ζ_0 and plotted for various dimensionless rotating speeds Rw. From the results, it can be seen that the smaller the flow rate or the higher the rotating speed, the greater the loss becomes. When the rotating speed is reduced to $\mathrm{Rw} = 0.9 \times 10^3$, however, the ratio ζ/ζ_0 becomes unity over the whole range of Re, not showing any effects of the rotation. In figure 5(a),

†The value Ro is calculated here based on the relative velocity and hydraulic diameter at the impeller inlet.

the results obtained by Murakami & Kikuyama (1972) are also plotted by — — — lines for the cases of $Rw = 2 \times 10^3$, 5×10^3 and 1×10^4. They show almost the same tendency as those for the present study except for the lower rotating speed $Rw = 2 \times 10^3$.

The results for the channel with the downward exit plotted in figure 5(b) show the same tendency as for the upward exit. The value of ζ/ζ_0, however, is larger than that for the upward exit and its maximum is about 3.4 times that of the upward exit. This greater sensitivity to the rotation is a disadvantage in the channel with the downward exit, though less so in a stationary state (figure 4).

As described above, the ratio ζ/ζ_0 is related to Re and Rw, suggesting that the results are closely related to Ro, which is the ratio of Re to Rw. Such a relationship between ζ/ζ_0 and the inverse of Ro, 1/Ro, is confirmed with the same data in figure 6, where the results for the upward exit, plotted with various symbols, are seen to fall on a single curve. When the flow rate decreases or the rotating speed increases, namely where 1/Ro increases, the ratio ζ/ζ_0 becomes greater than unity in the range $1/Ro > 0.08$ and increases progressively with increasing 1/Ro, reflecting the remarkable effect of rotation. For the channel with a downward exit it is also expressed with a single curve, as plotted by the — — — line in figure 6. This result, however, begins to increase at a lower value of 1/Ro ($1/Ro = 0.035$) than for the upward exit, and increases more rapidly. The results of Murakami & Kikuyama (1972), shown by the – – – line, increase rapidly when $1/Ro > 0.09$.

In consideration of the similarity to impeller flows, we find that the results for the channel with an upward exit are more affected by the inlet curvature (figure 4) and less by the rotation (figure 6). In what follows, impellers show excessive losses, such as inlet shock loss and the loss due to the curved passage, and the effect caused by the rotation is expected to be relatively small.

3.2. Hydraulic loss in air–water two-phase flow

When the mixture flows in a stationary channel, the relationship between the pressure-loss multiplier ϕ_{L0}^2 and Re is expressed as a function of the inlet void fraction ϵ_0, as shown in figure 7. When the void fraction is as small as $\epsilon_0 \leqslant 0.009$, the value ϕ_{L0}^2 nearly equals unity in almost the whole range of Re. This shows that the loss is not affected by the existence of the gas phase. When ϵ_0 is greater, however, the curve ϕ_{L0}^2 shifts upward in parallel and the value ϕ_{L0}^2 increases rapidly with a decrease in Re for the range $Re < 2.5 \times 10^4$.

When the channel is rotated, the pressure-loss multiplier ϕ_L^2 increases with increasing ϵ_0, as shown in figure 8, in which the results for various Rw and Re values are plotted. The top of figure 8 gives the results for the lower rotating speed of $Rw = 3 \times 10^3$. The value ϕ_L^2 for the smaller flow rate of $Re = 2.5 \times 10^4$ increases with the increase in ϵ_0, but it remains almost unaltered when $\epsilon_0 \geqslant 0.05$. At the larger flow rates of $Re = 3 \times 10^4$ and 3.5×10^4, the values of ϕ_L^2 nearly equal unity, being unaffected by ϵ_0, but they increase in the range $\epsilon_0 > 0.04$ and take almost the same value as that for $Re = 2.5 \times 10^4$ when $\epsilon_0 > 0.07$.

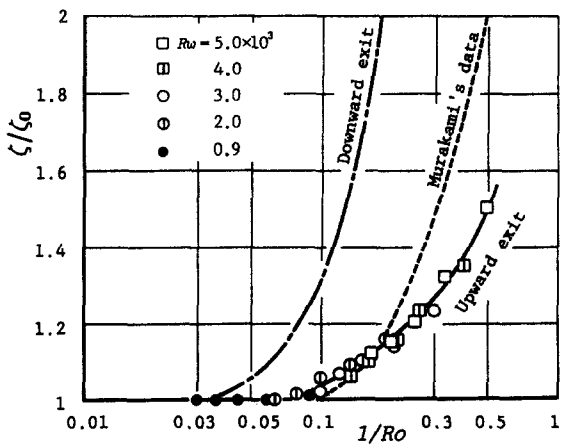

Figure 6. Relationship between 1/Ro and the friction factor ratio ζ/ζ_0 under single-phase water flow conditions.

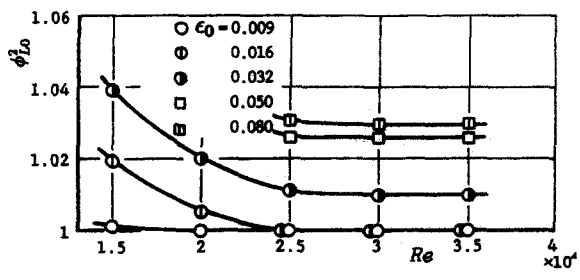

Figure 7. Pressure-loss multiplier for the stationary channel ϕ_{L0}^2.

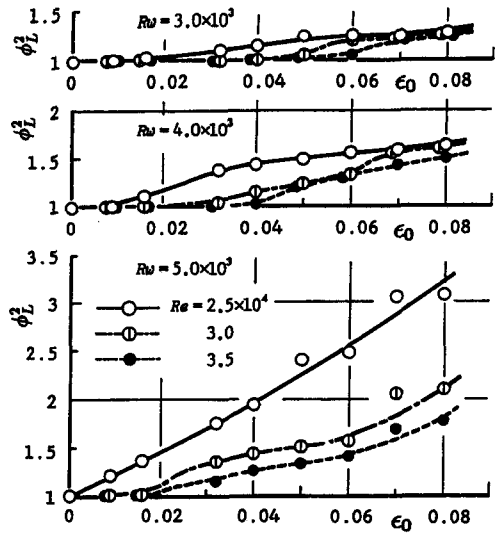

Figure 8. Relationship between ϵ_0 and the pressure-loss multiplier for the rotating channel ϕ_L^2.

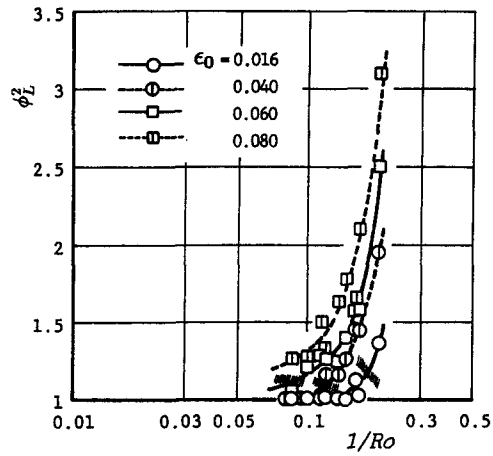

Figure 9. Relationship between 1/Ro and the pressure-loss multiplier ϕ_L^2.

The middle section of figure 8 shows the results for the higher rotating speed of $Rw = 4 \times 10^3$. ϕ_L^2 increases more rapidly with an increase in ϵ_0. With a decrease in Re, ϕ_L^2 begins to increase at a smaller value of ϵ_0. The bottom section of figure 8 shows the results for the highest rotating speed of $Rw = 5 \times 10^3$. ϕ_L^2 increases more rapidly. Consequently, the smaller the flow rate of water or the higher the rotating speed (i.e. the larger the 1/Ro value), the greater the loss ϕ_L^2 becomes, even in two-phase flow conditions.

Figure 9 shows the relationship between ϕ_L^2 and 1/Ro for various values of ϵ_0. The value ϕ_L^2 equals unity in the lower range of 1/Ro and increases sharply when 1/Ro is increased beyond a certain value, similar to the relationship between ζ/ζ_0 and 1/Ro for the single-phase flow (figure 6). When ϵ_0 is increased, the curve of ϕ_L^2 shifts upward in parallel and shows a rapid increase at the lower value of 1/Ro. The bands in figure 9 indicate the flow regime boundary described later (in figure 15), where the bubbly flow changes into slug flow as the value of 1/Ro increases. These bands, therefore, reflect the point where the homogeneous assumption implicit in the way the velocity W_{tp} is evaluated is no longer valid, owing to the existing velocity difference between the two phases.

When the loss for the rotating channel ϕ_L^2 shown in figure 9 is divided by that for the stationary one ϕ_{L0}^2, the resultant ϕ_L^2/ϕ_{L0}^2 represents the effect of the rotation, as shown in figure 10, where the results for $\epsilon_0 = 0.032$ are plotted with different symbols for various Rw and those for the different values of ϵ_0 are represented by various lines. When $1/Ro < 0.1$, the ratio ϕ_L^2/ϕ_{L0}^2 nearly equals unity, being the same as that for the stationary pipe. When 1/Ro is increased beyond the limit, the ratio begins to increase, at a greater rate with increasing ϵ_0.

3.3. Pressure distributions in the radial direction

Since losses under two-phase flow conditions change in accordance with Ro, as described in figures 9 and 10, the related distributions of the pressure $\Delta\psi_r$ in the radial direction are also changed in accordance with Ro, as shown in figure 11 where the results on the front (P.S.) and back (N.S.) sides for various ϵ_0 are shown by the symbols ○ and □, respectively.

When 1/Ro is only 0.086, the effects of the rotation and ϵ_0 are slight and the value of $\Delta\psi_r$ on the front side is higher than on the back side, due to the Coriolis force shown at the top in figure 11. In this figure, the idealized pressure rise for inviscid single-phase flow is indicated by the — — — line, which almost parallels the experimental results, and a remarkable loss arises mainly in the inlet elbow. For small $\epsilon_0 \leqslant 0.05$, the distributions on the front side remain almost unchanged, and those on the back side shift downward in parallel. Even when $\epsilon_0 = 0.08$, the distribution curves are still parallel, though they are shifted downward. This suggests that the entrained air is easily discharged from the channel, owing to an inertial force of flow greater than the Coriolis force; i.e. the internal flow conditions remain substantially unaltered.

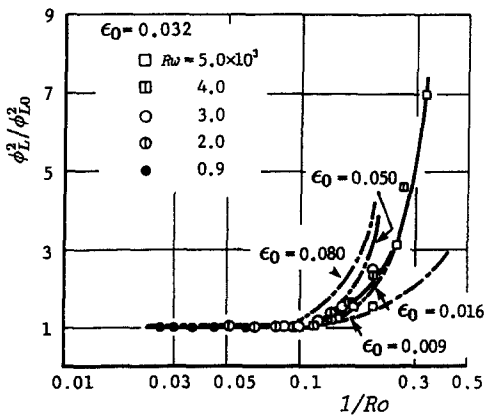

Figure 10. Relationship between 1/Ro and the pressure-loss multiplier ratio ϕ_L^2/ϕ_{Lo}^2.

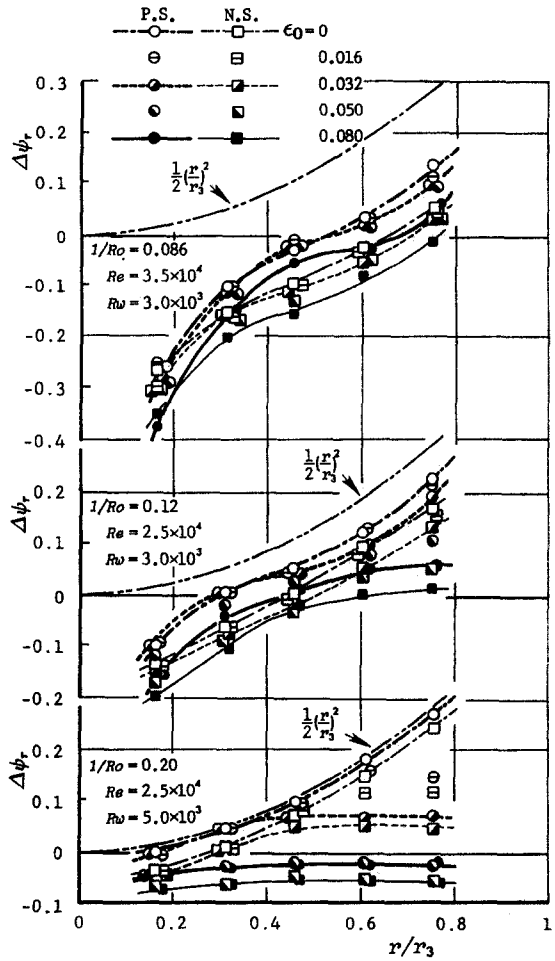

Figure 11. Pressure distributions in the radial direction.

When 1/Ro exceeds a certain value, the loss under the two-phase flow conditions increases rapidly as described. When the results are slightly greater than the limit (1/Ro = 0.12), they are as plotted in the middle section of figure 11. For a smaller value of ϵ_0, such as $\epsilon_0 \leqslant 0.032$, $\Delta\psi_r$ in the rear half of the channel decreases more, but the distributions are similar to those for 1/Ro = 0.086 (top of figure 11). For a larger value, $\epsilon_0 \geqslant 0.05$, however, $\Delta\psi_r$ decreases greatly in the outlet region ($r/r_3 \geqslant 0.61$) and the pressure rise in the radial direction is almost nil. In this range of ϵ_0 there exists a predominant region of high void fractions near the outlet, as described in the next section, and a greater loss of pressure is brought about in this lower density region.

When 1/Ro is increased to 1/Ro = 0.2, the results are greatly affected by ϵ_0 as shown at the bottom of figure 11. Owing to a small flow rate of water, the loss in the inlet elbow is so little that the pressure distribution under the single-phase flow is almost the same as the ideal one. Even for small ϵ_0, however, the pressure rise is less in the downstream region, which expands upstream with the increase in ϵ_0. This is attributable to the change in the flow conditions described in the next section.

The pressure distributions in two horizontal sections displaced upward and downward ($z/a = 0.19$, 0.81) show changes similar to those indicated in figure 11 ($a/z = 0.5$), so they are not displayed here. But near the outlet in the upper section ($z/a = 0.81$), $\Delta\psi_r$ becomes less due to the increase in ϵ.

3.4. Distributions of the void fraction

The hydraulic loss as well as the pressure distribution in the channel is closely related to the flow conditions, as discussed from the standpoint of the distributions of void fraction in the following.

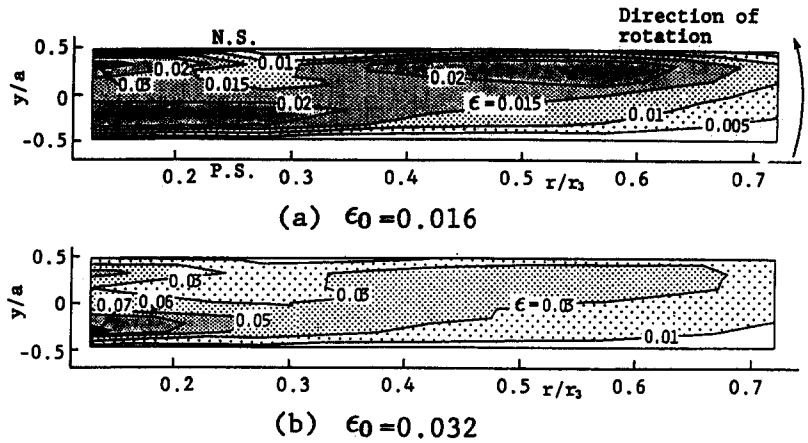

Figure 12. Distributions of void fractions for high Ro (1/Ro = 0.086).

From measured void fractions ϵ on a central section between the bottom and top of the horizontal channel ($z/a = 0.5$), contour lines of ϵ† are obtained as illustrated in figures 12–14, where the coordinate axes are a dimensionless radial coordinate r/r_3 and a dimensionless width coordinate y/a, respectively, and the values of $y/a = -0.5$ and 0.5 correspond to the front (P.S.) and back (N.S.) sides of the channel, respectively.

When 1/Ro is small, 1/Ro = 0.086, the distribution is rather uniform over the whole channel, as seen in figure 12. The results for $\epsilon_0 = 0.016$, plotted in figure 12(a), show a so-called saddle-type distribution in the inlet region ($0.13 \leqslant r/r_3 \leqslant 0.33$); thus, the value of ϵ becomes lower in the center of the passage. Such a distribution is also observed for upward bubbly flows in stationary vertical pipes, which accounts for the effect of the lift force generated by the relative velocity between two phases (Rouhiainen & Stachiewicz 1970). The distribution obtained in this experiment, however, is considered attributable to the fact that air bubbles are caught in a pair of vortexes induced by the secondary flow due to the curvature of the inlet elbow. In the downstream region, however, the saddle-type distribution disappears and the value ϵ increases on the back side. This is attributable to the fact that the bubbles shift toward the back side from the front in the course of the flow, owing to the pressure gradient produced by the Coriolis force. Figure 12(b) shows the results for $\epsilon_0 = 0.032$. Although the value ϵ is increased near the front of the inlet, its maximum is $\epsilon/\epsilon_0 = 2$ at most, and it maintains a rather uniform distribution.

When 1/Ro is larger, 1/Ro = 0.12, the distributions depend on the inlet void fraction ϵ_0 as shown in figure 13, where the results for $\epsilon_0 = 0.016$, 0.032 and 0.05, 0.08 are indicated. When $\epsilon_0 \leqslant 0.032$, the distributions are seen to be similar to the case in figure 12. With an increase in ϵ_0, however, the value ϵ near the downstream back side increases progressively. A void region of $\epsilon \geqslant 0.9$, as well as predominating region of high void fractions of $\epsilon \geqslant 0.6$, appears and spreads upstream into the inlet when $\epsilon_0 \geqslant 0.5$. As these regions were measured almost consistently, the flow regime is supposed to be changed there from bubbly flow into slug flow. In this predominant region ($\epsilon \geqslant 0.6$) the pressure ceases to increase in a radial direction, as seen in the middle of figure 11. Although the illustration is omitted, the value ϵ near the top side of the channel becomes higher in the downstream direction, because the bubbles shift vertically upward due to buoyancy.

Figure 14 shows the results for the much greater 1/Ro = 0.2. Even at small $\epsilon_0 = 0.016$, there is a dominating region of high void fractions ($\epsilon \geqslant 0.6$) near the back side in the region $r/r_3 \geqslant 0.52$, where nil pressure arises in a radial direction (see the bottom section of figure 11). Although such a dominating region was observed consistently at $\epsilon_0 = 0.016$, under strobolighting the region appears to oscillate in the radial direction when $\epsilon_0 \geqslant 0.032$; the time cycle of the oscillation was smaller than the inverse of the angular velocity of the rotating channel $1/\omega$.

†To draw the contour lines of void fractions ϵ, 48 triangular elements, with vertexes corresponding to 35 measuring points for void fractions, were constructed. A linear interpolation method was then applied on each side of a triangle to obtain the point of equi-void fraction.

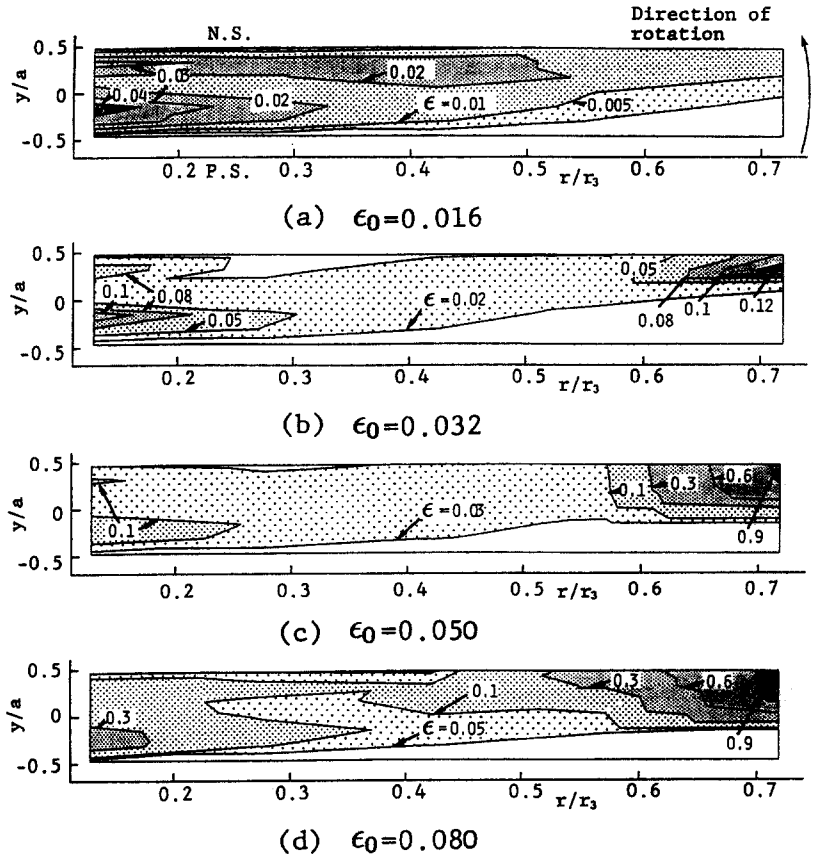

Figure 13. Distributions of void fractions for medium Ro (1/Ro = 0.12).

According to the analytical model for the flow regime transitions by Taitel & Dukler (1976), gas–liquid two-phase flows in horizontal and inclined pipes are mapped with a solid line for the dispersed bubble and intermittent (slug and plug) regions shown in figure 15, where the coordinate X is the so-called Lockhart–Martinelli parameter ($= [(dp/ds)_L/(dp/ds)_G]^{1/2}$) and the coordinate T is a characteristic number of gravity, defined as the ratio of turbulent to gravity forces acting on the gas as $T = [|(dp/ds)_L|/(\rho_L - \rho_G)g \cos\alpha]^{1/2}$, where α is the inclined angle of the pipe. As this model takes the gravity effects into consideration, the rotating effects of pipes could also be predicted by using the Coriolis acceleration $2\omega W_L$ instead of the gravity one $g \cos\alpha$. The flow regimes observed in this experiment are denoted for the homogeneous bubbly flow regime by ○, △, ⬡, ◇ and ▽, and for the slug flow with predominant regions of high void fraction ($\epsilon \geqslant 0.6$) by ◆, ▼ and ■. This transition boundary is seen to increase somewhat greater than the predicted one as shown by the ––– line.

When 1/Ro is larger, when the rotating speed is high and the liquid flow rate is small, a predominant region of high void fractions appears on the back side near the outlet, as described above. This is confirmed to be the region accumulating bubbles, as shown in photographs ($0.05 < 1/\mathrm{Ro} < 0.12$) by Patel & Runstadler (1978). They also conducted an experiment on a mixed-flow pump ($0.6 < 1/\mathrm{Ro} < 1.0$), and the void spread over all the impeller was observed when $\epsilon_0 \geqslant 0.071$ (Patel & Runstadler 1978). According to our own experimental results in a radial-flow impeller (Murakami & Minemura 1974), a dominating region of high void fractions was observed near the back side of the blade in the inlet when $0.21 \leqslant 1/\mathrm{Ro} \leqslant 0.36$ and $0.04 \leqslant \epsilon_0 \leqslant 0.075$, and a void was observed over the whole back side when $0.47 \leqslant 1/\mathrm{Ro} \leqslant 0.62$ and $0.07 \leqslant \epsilon_0 \leqslant 0.09$. This demonstrated a close relation with the present rotating channel at identical Ro.

4. CONCLUSIONS

A straight pipe having a square section is mounted radially on a horizontal disk and rotated around its vertical axis under two-phase flow conditions. The related hydraulic loss as well as the

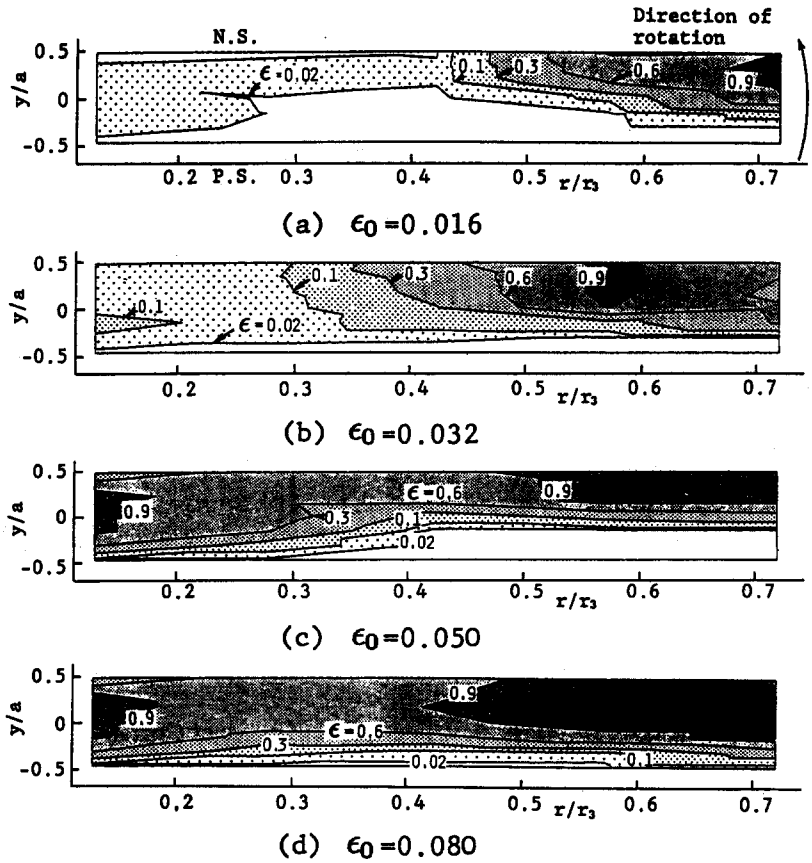

Figure 14. Distributions of void fractions for low Ro (1/Ro = 0.2).

distributions of pressure and void fraction were measured under a bubbly flow regime. The results obtained are summarized as follows:

(1) Under single-phase liquid flow conditions, the friction factor for the stationary channel ζ_0 decreases with an increase in Re, and becomes constant when $Re \geqslant 2.5 \times 10^4$. The resultant loss ratio ζ/ζ_0 of the rotating channel ζ to the stationary one ζ_0 is represented by a single curve for 1/Ro, and increases progressively from unity when 1/Ro exceeds a certain limit (1/Ro $\simeq$ 0.88 for the upward exit).

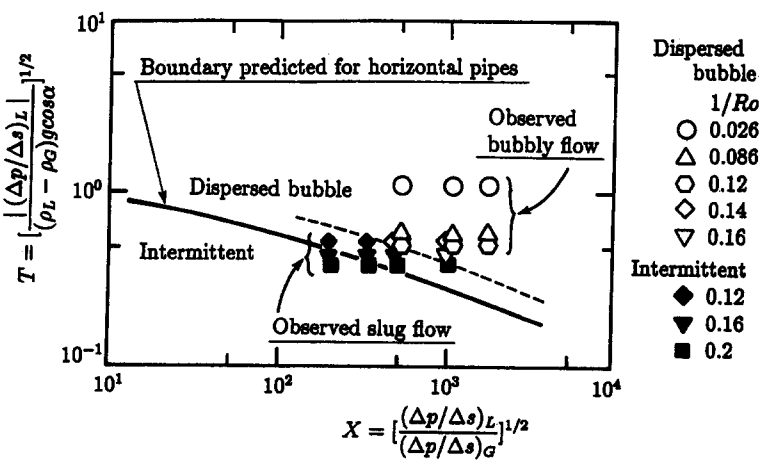

Figure 15. Flow regime map by Taitel & Dukler (1976).

(2) The pressure-loss multiplier for the stationary channel ϕ_{L0}^2 increases with an increase in ϵ_0. When Re is increased, ϕ_{L0}^2 decreases and becomes constant in the range $Re \geqslant 3 \times 10^4$.

(3) When ϵ_0 is constant, the relationship between 1/Ro and the pressure-loss multiplier for the rotating channel ϕ_L^2 falls on a single curve and increases sharply when 1/Ro exceeds a certain limit ($1/Ro \simeq 0.1$). The greater the value ϵ_0, the greater the value ϕ_L^2 becomes, and ϕ_{L0}^2 begins to increase sharply with a lower value of 1/Ro.

(4) When 1/Ro is small ($1/Ro \leqslant 0.1$), the radial pressure rise on the front side remains almost unaltered and that on the back side decreases in parallel in the range $\epsilon_0 \leqslant 0.05$. The distributions of void fractions are hardly affected by ϵ_0. When 1/Ro is greater, predominant regions of high void fractions appear in the inlet ($r/r_3 \leqslant 0.02$) and outlet ($r/r_3 \geqslant 0.45$), and they expand with increasing ϵ_0. In such regions the pressure hardly rises in the radial direction.

(5) The flow regime boundary for the bubble flows in the rotating channel can be approximately estimated with Taitel & Dukler's (1976) mapping method using Coriolis acceleration ($2\omega W_L$) instead of the gravity one ($g \cos \alpha$).

REFERENCES

MINEMURA, K. & MURAKAMI, M. 1988 Developments in the research of air–water two-phase flows in turbomachinery. *JSME Int. J. Series II* **31,** 615–622.

MURAKAMI, M. & KIKUYAMA, K. 1972 Pipe flow under the influence of Coriolis forces. *Bull. JSME* **15,** 747–758.

MURAKAMI, M. & MINEMURA, K. 1974 Effects of entrained air on the performance of a centrifugal pump (1st Report: performance and flow conditions). *Bull. JSME* **17,** 1047–1055.

PATEL, B. R. & RUNSTADLER, P. W. 1978 Investigations into the two-phase flow behavior of centrifugal pumps. In *Proceedings of Polyphase Flow in Turbomachinery*, pp. 79–100. ASME, New York.

ROUHIAINEN, P. O. & STACHIEWICZ, J. W. 1970 On the deposition of small particles from turbulent streams. *Trans. ASME Ser. C* **92,** 169–177.

TAITEL, Y. & DUKLER, A. E. 1976 A model for predicting flow regime transitions in horizontal and near horizontal gas–liquid flow. *AIChE Jl* **22,** 47–55.

ZAKEM, S. 1980a Determination of gas accumulation and two-phase slip velocity ratio in a rotating impeller. In *Proceedings of Polyphase Flow Transport Technology*, pp. 167–173. ASME, New York.

ZAKEM, S. 1980b Analysis of gas accumulation and slip velocity in a rotating impeller. In *Proceedings of a Cavitation and Polyphase Flow Forum*, pp. 32–34. ASME, New York.